Macromolecules

pubs.acs.org/Macromolecules Article

Compatibilizing Immiscible Polymer Blends with Sparsely Grafted Nanoparticles

Husam Alkhodairi, Sebastian T. Russell, Julia Pribyl, Brian C. Benicewicz, and Sanat K. Kumar*

Cite This: *Macromolecules* 2020, 53, 10330−10338 Read Online

ACCESS | Metrics & More | Article Recommendations | Supporting Information

ABSTRACT: The use of nanoparticles (NPs) to compatibilize immiscible polymer blends remains an ongoing challenge requiring a high level of control over the NP dispersion and localization. Here, we show that silica NPs "sparsely" grafted with long polystyrene (PS) chains are surfactant-like because they permit core−core, core−matrix, and corona−matrix interactions. When placed at an immiscible polymethyl methacrylate (PMMA)−PS interface, the silica core strongly interacts with one component (PMMA), while the corona mixes with the other (PS). These carefully designed NPs are demonstrated to be efficient stabilizers, even outperforming block copolymers. While such surfactant-like behavior is evident, and understood on the basis of existing ideas, a new concept that we leverage is how the shape of the interfacial free energy profile is affected by the surface grafting density. For an optimally chosen grafting density and graft chain length, we find a nearly symmetric free energy profile as a function of the NP contact angle at the interface, ensuring that the NPs are strongly localized in a region where they are the most efficient in terms of stabilization.

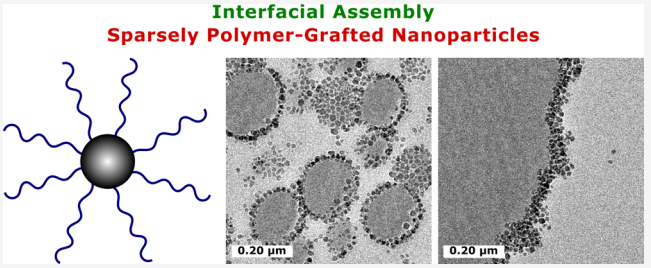

INTRODUCTION

Polymer blending is a convenient technique for combining the desirable properties of different polymers into a hybrid material. However, most polymer blends are thermodynamically immiscible because of their unfavorable enthalpic interaction and the low entropy of mixing of long-chain molecules. They are therefore dominated by poor interfacial adhesion and unstable morphologies that are frequently associated with the formation of large domains—shortcomings that pose challenges in the processing of these materials and in their end-use (mechanical) performance. Several compatibilization strategies have been introduced to overcome these issues;[1] the most frequent one being the use of premade or *in situ*-generated block copolymers.[2−9] Because of their amphiphilic character, these block copolymers (i) self-assemble at polymer−polymer interfaces, (ii) minimize domain coalescence, and (iii) improve the interfacial adhesion between the components.[10] Thus, any potential compatibilizer must meet or exceed these requirements to produce materials having improved processability and mechanical properties.

Recently, interfacially active nanoparticles (NPs) have been suggested as potential alternatives to blends compatibilized with block copolymers.[11−24] This is partly motivated by their higher adsorption energy, which makes their displacement from the polymer−polymer interface a high energy process, leading to reduced domain coalescence.[25] Unfortunately, their use in polymer media requires special techniques to prevent them from aggregating and macrophase-separating from the matrix polymers.[26] In the context of immiscible polymer systems, they must also be tuned to localize them at the interface. The most promising strategy involves attaching molecular[27−31] or macromolecular[11−18,32−42] ligands to their surfaces, which act to control the NP location within the blend and also minimize NP aggregation by steric repulsion.

NPs in Polymer Blend Matrices. Composto and coworkers[16] investigated the segregation behavior of 12.8 nm diameter silica NPs grafted with chlorine-terminated polymethyl methacrylate (PMMA) (PMMA-*g*-SiO_2) in blends of PMMA/poly(styrene-*r*-acrylonitrile) (SAN). The NPs had a fixed grafting density (σ) of 0.7 chains/nm^2, while the PMMA graft molecular weight (M_n) varied systematically from 1.8 to 160 kDa—thus probing various melt to graft chain length ratios ($1/\alpha$; see Figure 1). They found that the NPs are dispersed in the PMMA matrix at the higher M_n (lower $1/\alpha$) end while becoming progressively more interfacially active with decreasing M_n (increasing $1/\alpha$). At such high grafting density, the NP surface is completely shielded by the PMMA brush.[44] Therefore, these workers ascribed this interfacial segregation to enthalpic and entropic effects stemming from the higher density of PMMA-unfavorable chlorine end groups and the

Received: September 14, 2020
Revised: November 8, 2020
Published: November 25, 2020

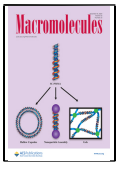

https://dx.doi.org/10.1021/acs.macromol.0c02108
Macromolecules 2020, 53, 10330−10338

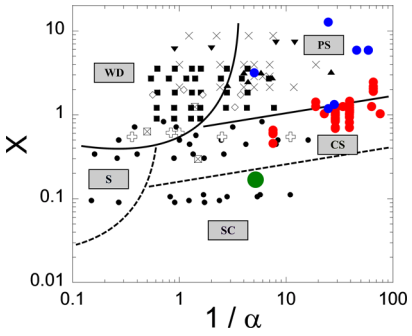

Figure 1. Dispersion of homopolymer-grafted NPs in a homopolymer matrix (black symbols), compiled by Kumar et al. in ref 43 from experimental data in the literature (WD: well-dispersed, PS: phase-separated, S: strings, CS: connected sheets, and SC: small clusters). The y and x axes represent the spherical brush overcrowding parameter (x) and the melt to brush chain length ratio ($1/\alpha$), respectively. On the same plot, we overlay the literature data for the interfacially active homopolymer- and block copolymer-grafted NPs in the immiscible polymer blend (blue symbols; refs [14−18]) and block copolymer matrices (red symbols; refs [34−40]). The green circle corresponds to the primary system investigated in this work.

pronounced autophobic dewetting (i.e., the exclusion of the chemically identical free polymer chains from the brush[45−47]), respectively, in the limit of low graft M_n. However, they also obtained interfacially active NPs with a hydrogen-terminated PMMA brush analogue, although they exhibited a relatively weaker interfacial activity. Thus, it appears that autophobic dewetting is a major factor in the interfacial segregation of these densely grafted NPs.

Similarly, some workers compatibilized PMMA/polystyrene (PS)[11,12] and poly(2,6-dimethyl-1,4-phenylene ether)/SAN[13] immiscible polymer blends by employing Janus NPs consisting of polybutadiene (PB) cores coated with PS and PMMA (brush) hemispheres. This was achieved by cross-linking the middle PB blocks in poly(styrene-*b*-butadiene-*b*-methyl methacrylate) (PS-*b*-PB-*b*-PMMA) triblock copolymers. However, despite some recent progress,[48] the large-scale fabrication of Janus NPs remains difficult relative to the well-established grafting methods.[49,50] They are therefore not the subject of this work.

NPs in Block Copolymer Matrices. Kramer and co-workers investigated the segregation behavior of small (d < 5 nm core diameter) gold NPs densely grafted with either homopolymers,[34−37] a mixture of homopolymers,[32,33] or copolymers[35,37,39,40] in poly(styrene-*b*-2-vinylpyridine) (PS-*b*-P2VP) diblock copolymer matrices. They investigated a range of grafting density ($\sigma \sim 0.4-4$ chains/nm^2) and graft molecular weight ($M_n \sim 1.5-13$ kDa). These workers found that PS-grafted NPs (PS-*g*-Au) localize in the PS domains for σ > 1.6 chains/nm^2, while they segregate to the PS−P2VP interface for σ < 1.3 chains/nm^2.[34] They attributed this transition to a more favorable P2VP−Au interaction relative to that of PS−Au. Nevertheless, such densely grafted NPs are not truly "surfactants" because the brushes would have minimal conformational freedom to allow the free polymers to have easy access to the surface, which, in turn, lowers the NP adsorption energy at the interface.

Overall Understanding. Kumar et al.[43] summarized the literature data for the dispersion of homopolymer-grafted NPs in a homopolymer matrix in a plot of the planar brush overcrowding parameter $\sigma N^{0.5}$ against $1/\alpha$. Here, we replot the data using x (Figure 1; black symbols), the curved brush analogue of this overcrowding parameter, which represents the ratio of the number of grafted chains to the number of chains that occupy the same volume in an unperturbed melt.[51] Thus, $x \ll 1$ and $x \gg 1$ correspond to the grafted NPs being star-like and strongly stretched, respectively. In the limit of high grafting density ($x \gg 1$), core−core attractions are screened, and only two dispersion states exist: well-dispersed (wet-brush regime) and phase-separated (dry-brush regime), with the crossover occurring for $1/\alpha \sim 4-6$. At intermediate grafting density, self-assembled structures appear, with strings forming for low $1/\alpha$ and connected sheets for high $1/\alpha$—these structures are the result of a competition between core−core attractions and the entropy of distorting the grafted chains.[26] On the same plot, we summarize the literature data for the interfacially active homopolymer- and block copolymer-grafted NPs in immiscible polymer blend (blue symbols) and block copolymer (red symbols) systems. Clearly, all the studies on the use of polymer-grafted NPs in polymer blends lie in the dry-brush regime, where autophobic dewetting effects are dominant, while most block copolymer studies are concentrated near the phase-separated−connected sheets boundary in the high $1/\alpha$ region.

Although these highly grafted NPs have indeed been found to improve the stability of immiscible homopolymer blends,[18,38] they suffer from several important limitations. First, the dense brush limits the extent of favorable interactions between the melts and the NP surface, such as the strong hydrogen-bonding interactions between PMMA and silica.[52] Moreover, the interpenetration between the brush and the melt is minimized in the high $1/\alpha$ regime at high grafting density.[53] These effects reduce the NP adsorption energy at the interface, which in turn reduces the stability of the compatibilized blend. They also result in poor adhesion between the two components, a necessary requirement for obtaining good mechanical properties.[10] Second, a positive interfacial tension exists between the brush and the chemically identical melt in the dry-brush regime,[45−47] leading to brush−brush attraction and aggregation to remove the unfavorable brush−melt interfaces.[54] This interfacial tension manifests itself in the abrupt transition from well-dispersed to phase-separated structures at high x with increasing $1/\alpha$. It is also probably responsible for the transition from the one-dimensional strings to the two-dimensional sheet morphology at intermediate x (Figure 1). Such aggregation is particularly problematic for melt mixing because a significant portion of these brushes will get incorporated in aggregates, thus preventing them from reaching the interface. Evidence of this can be seen in the PMMA/SAN blends investigated by Composto et al.,[16] which exhibit a lower critical solution temperature-type phase behavior. Their as-cast morphologies show one-phase mixtures with homogeneously distributed NPs; however, after annealing at 195 °C for 24 h, the blends phase-separated, and large NP aggregates are seen in the PMMA phase and at the interface. This limitation is analogous to the one presented by premade high-molecular weight block copolymer compatibilizers, which may become trapped in micelles in a bulk phase even at very low loadings.[5]

On the other hand, in the low x limit, both the cores and the coronas are easily accessible to the free polymers. It is precisely in this limit, where we believe the maximum NP "surfactancy," and thus stabilization effect, is obtained: the cores strongly interact with one free polymer and the coronas with the other.

https://dx.doi.org/10.1021/acs.macromol.0c02108
Macromolecules 2020, 53, 10330−10338

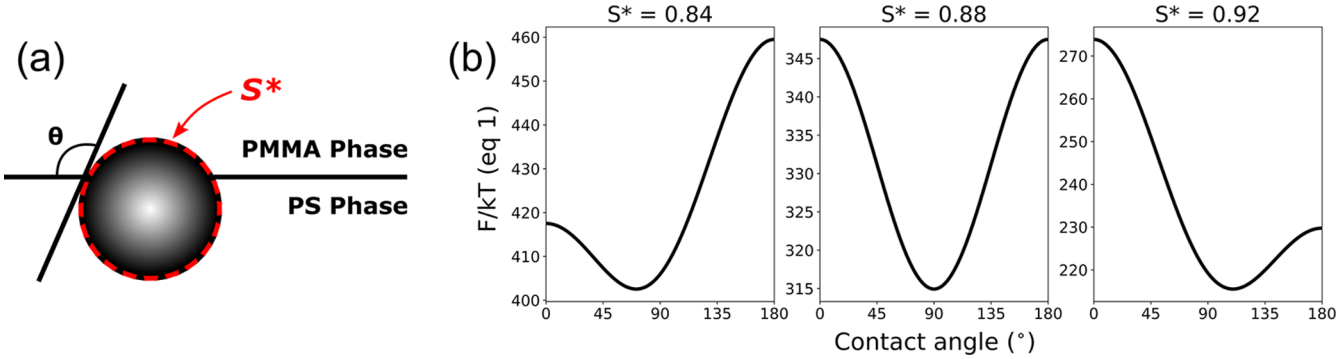

Figure 2. PS-grafted silica NP at the PMMA−PS interface where the red regions represent the excluded fraction of the silica surface (S^*) because of the presence of the grafts (a) and plots of the interfacial free energy (eq 1) normalized by kT for different surface coverages S^* (b).

Motivated by these ideas, here, we consider the stabilization efficiency of PS-grafted spherical silica NPs (PS-*g*-SiO_2) of core diameter d = 14 nm, grafting density σ = 0.02 chains/nm^2, and graft molecular weight M_n = 110 kDa, in a PMMA/PS immiscible polymer blend. A simple geometric argument[51] shows that these grafting densities are low enough that both the cores (which have a more favorable interaction with the PMMA[52]) and the coronas (whose miscibility with the PS matrix can be tuned) are accessible to the matrix polymers. Thus, these surfactant-like NPs combine the dual advantage of being selectively localized at the interface while being hard to displace from this zone. We show that the resulting morphologies remain stable even after 25 days of annealing at 190 °C, demonstrating the effectiveness of these NPs as compatibilizers.

Localization Free Energy. Consider a spherical silica NP sparsely grafted with PS chains adsorbed at a planar PMMA−PS interface. The graft conformations are likely to be asymmetric across the interface because of the different brush−melt interaction parameters χ and $1/\alpha$ ratios, coupled with the low grafting density, which permits conformational freedom for the grafts. However, for simplicity, we assume that the grafts are uniformly distributed across the interface, and that they work to shield a fraction S^* of the silica surface (Figure 2a).[44] If we also neglect line tension, then the interfacial free energy attributed to placing this NP at the interface is

$$F = (\gamma_{1C}A_1 + \gamma_{2C}A_2)(1 - S^*) + (\gamma_{1B}A_1 + \gamma_{2B}A_2)(S^*) - \gamma_{12}A_{12} \quad (1)$$

where γ_{ij} is the interfacial tension between the ith and jth components (1 = PMMA, 2 = PS, B = brush, C = silica). The first two terms represent the free energy associated with the contacts of the cores and the coronas with the two free polymers, while the last term corresponds to the elimination of an area A_{12} of the PMMA−PS interface by the particle. The areas are given by

$$A_1 = 2\pi r^2(1 + \omega); \qquad A_2 = 2\pi r^2(1 - \omega);$$
$$A_{12} = \pi r^2(1 - \omega^2)$$

where r is the NP radius, $\omega = \cos\theta$, and θ is the NP contact angle at the interface (Figure 2a). The equilibrium ω can be obtained by minimizing eq 1 with respect to θ, yielding

$$\omega = \frac{(\gamma_{2C} - \gamma_{1C})(1 - S^*) + (\gamma_{2B} - \gamma_{1B})(S^*)}{\gamma_{12}} \quad (2)$$

The particle localizes at the interface for $-1 < \omega < 1$, while for $\omega < -1$ and $\omega > 1$, it is preferentially located in the bulk PS or the bulk PMMA, respectively. Because of the lack of experimental data, the silica−PMMA (γ_{1C}) and silica−PS (γ_{2C}) interfacial tensions were calculated using the Owens−Wendt method[55] (see Supporting Information). It was found that γ_{1C} = 12.86, γ_{2C} = 19.18, and γ_{12} = 0.87 mN/m. The last number is in close agreement with that obtained by experimental measurements.[56] Note that for S^* = 0 (corresponding to an ungrafted NP), eq 2 reduces to the well-known Young's equation and gives ω = 7.26. Thus, the bare silica NP prefers to be in the PMMA phase. This is expected because the hydroxyl groups on the silica surface form hydrogen-bonding interactions with the carbonyl groups of the PMMA.[52] At the other end of the spectrum, with S^* = 1 (corresponding to a densely grafted NP), ω reduces to $(\gamma_{2B} - \gamma_{1B})/\gamma_{12}$, that is, the core plays no role in the NP segregation, similar to the Composto et al.[16] work discussed earlier. The numerator of eq 2 can be manipulated through modulating S^* by varying σ and the graft M_n to obtain the desired wetting parameter ω.[44]

We now consider the interfacial tensions between the PS brush and the two free polymers. When the brush and the free polymer are chemically nonidentical, this interfacial tension is a combination of enthalpic and entropic components. Hence, in principle, the PMMA−brush (γ_{1B}) and the PS−brush (γ_{2B}) interfacial tensions are greater than γ_{12} and zero, respectively, with the magnitudes increasing with increasing $1/\alpha$.[57,58] However, as Archer and co-workers[53] point out, polymer brushes attached to "curved" surfaces exhibit a broad wet brush regime, with the dewetting crossover being largely independent of σ and occurring for $1/\alpha \sim 4$−6 (compared to $1/\alpha \sim 1$ for flat brushes). Thus, even in the dry brush regime, the interface between the brush and the free homopolymer is not a sharp one for long enough grafts, and some degree of mixing occurs near the free ends of the brush because of reduced brush crowding in that region. Therefore, for the conditions that we probe here, the entropic contributions to γ_{1B} and γ_{2B} are negligible, and the difference $(\gamma_{2B} - \gamma_{1B})$ in eq 2 is dominated by γ_{1B}. Hence, in the following, we set $\gamma_{1B} = \gamma_{12}$ and $\gamma_{2B} = 0$.

The wetting equation (eq 2) suggests that an interfacially active band ($0° \le \theta \le 180°$) exists for the PMMA/PS/PS-*g*-SiO_2 system between $S^* \approx 0.76$ and $S^* \approx 1.00$. (Because the equation does not account for the thickness of the brush in the area terms, these bounds serve as a guide in designing the NP.)

https://dx.doi.org/10.1021/acs.macromol.0c02108
Macromolecules 2020, 53, 10330−10338

In this framework, the particle has a 90° contact angle (i.e., it equally wets both phases) when $S^* \approx 0.88$. A plot of the interfacial free energy (eq 1) as a function of θ for $r = 7$ nm reveals that this NP is trapped in a deep energy well of $\sim 32kT$ (Figure 2b). By comparison, the $S^* = 0.84$ and $S^* = 0.92$ coverages show asymmetric free energy profiles with a $\sim 15kT$ cost for them to desorb from the interface into the bulk PMMA or PS phases, respectively (Figure 2b). Thus, subtle changes in the grafting density and the graft chain length drastically affect the stabilization efficiency, emphasizing the importance of proper polymer-grafted NP design. To be clear, these three free energy profiles can still be in the sparse brush limit; for 14 nm diameter NPs, 110 kDa grafts, and S^* between 0.84 and 0.92, σ is between 0.017 and 0.025 chains/nm^2 and x is between 0.13 and 0.18, respectively.[44]

To calculate the polymer surface coverage S^*, we follow the models developed by Asai et al.[44] Briefly, each grafted chain is treated as a rigid equivalent sphere (ES) of radius R. The ESs are assumed to exclude a fraction S^* of the grafted NP surface, where another "bare" NP cannot contact. We use the approximation $R = 0.87R_g f^{-1/5}$, which we calculated from Asai et al.'s data for $r = 7$ nm PS-g-SiO$_2$ NPs, where $R_g \approx 0.5(N/6)^{1/2}$ and f is the number of grafts.[44] There are several combinations of σ and M_n for which $S^* \approx 0.88$. We anticipate that using long grafts will be advantageous for stabilization and (especially) for mechanical properties because the number of entanglements between the grafts and the matrix are maximized in the limit of high graft M_n.[10] Thus, we set $M_n = 110$ kDa, and we find $\sigma = 0.02$ chains/nm^2, giving $S^* \approx 0.87$.

EXPERIMENTAL DETAILS

Materials. Two PMMAs ($M_w = 75$ and 87 kDa, $M_w/M_n \sim 2$) and two nearly monodisperse PSs ($M_w = 32$ and 571 kDa, $M_w/M_n \approx 1.04-1.09$) were purchased from Scientific Polymer Products Inc. and used as received. Symmetric poly(styrene-b-methyl methacrylate) (PS-b-PMMA, $M_w^{total} = 104$ kDa, $M_w/M_n \approx 1.09$) was purchased from Polymer Source and used as received. PS-g-SiO$_2$ NPs (14 ± 4 nm core diameter) were synthesized using the reversible addition−fragmentation chain transfer polymerization process[50] (see Supporting Information for detailed instructions). Antioxidant Irganox 1010 was kindly donated by BASF. Tetrahydrofuran (THF, ACS reagent, ≥99.0%), toluene (ACS reagent, ≥99.5%), methanol (MeOH, ACS reagent, ≥99.8%), and 1-chloropentane (99%) were purchased from Sigma-Aldrich and Fisher Chemical. Silicon wafers (Si, 50.8 mm diameter) were purchased from University Wafer.

Preparation of PMMA/PS Bilayers. Si wafers were cleaved into 1 cm × 1 cm squares, washed in a sonicated MeOH bath, and finally plasma-cleaned to remove any remaining organics. The spin-coating procedure was performed as follows: (i) a ~600 nm PMMA film was spin-coated from a toluene solution, (ii) the PMMA film was dried under vacuum for 2 h, and (iii) a ~600 nm PS film was spin-coated from a 1-chloropentane solution, a selective solvent for PS. The bilayers were then allowed to float on water, picked up onto pre-prepared epoxy substrates, and annealed under vacuum for transmission electron microscopy (TEM) studies or annealed under vacuum and then immersed into a 1-chloropentane bath to remove the PS layer for atomic force microscopy (AFM) studies. Annealing was performed at 150 °C for 24 h.

Preparation of PMMA/PS Blends by Rapid Precipitation. Stock PMMA and PS solutions of concentration 60 mg/mL were prepared by dissolving in THF with 1.0 wt % Irganox 1010. PMMA/PS blends of composition 80/20 (w/w) were prepared by mixing the appropriate amounts from these stock solutions. The required loadings of the PS-g-SiO$_2$ (with respect to the silica core) and PS-b-PMMA compatibilizers (both dissolved in THF) were added to the PMMA/PS solutions. The solutions were then probe-ultrasonicated for 3 min (pulse mode; 2 s sonication, 1 s rest) with a model GEX-750 operated at 24% of the maximum amplitude. Separately, mechanically agitated MeOH baths (MeOH/THF = 250:1 by volume) were prepared.[59] The THF solutions were poured into the agitated MeOH baths dropwise with a syringe pump. The precipitated blends were collected and dried under vacuum at room temperature for 48 h to remove trace solvent and then annealed under vacuum at 190 °C for the designated period (up to as long as 25 days).

RESULTS AND DISCUSSION

Equilibrium Localization. Figure 3 shows TEM micrographs for PMMA/PS bilayers that are prepared by sequential spin-coating on silicon wafers with the NPs initially loaded into either the PS or the PMMA layers. This arrangement is designed to examine whether kinetic effects have any influence on the NP localization after annealing. Regardless of the initial layer, the NPs were placed in, the ungrafted NPs resided in the PMMA layer (Figure 3a), and the sparsely grafted ones localized at the interface (Figure 3b) upon annealing for 24 h at 150 °C. Moreover, the contact angle of the NPs at the bilayer interface was measured by AFM and was found to be 83 ± 11°. Thus, no measurable kinetic effects are observed in terms of NP localization, and the measured θ is as predicted by eq 2.

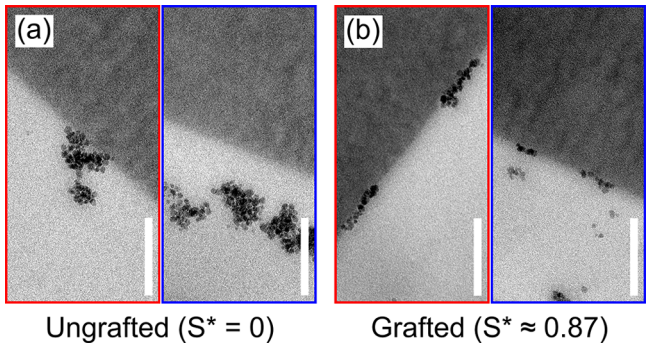

Figure 3. TEM micrographs showing the equilibrium localization of ungrafted (a) and sparsely PS-grafted ($\sigma = 0.02$ chains/nm^2, $M_n = 110$ kDa); (b) NPs in PMMA/PS bilayers after annealing at 150 °C for 24 h. Initially, the NPs were loaded into either the PS (red border) or the PMMA (blue border) layers. The molecular weights are 75 and 32 kDa for PMMA and PS, respectively. Brighter phase is PMMA, and darker one is PS. Scale bars are 200 nm.

Stabilization Efficiency in the Melt State. To probe the stabilization efficiency of these sparsely grafted NPs, we prepared bulk PMMA/PS blends loaded with 0.5 vol % NPs (with respect to the silica core). We choose an asymmetric 80/20 (PMMA/PS) blend ratio to allow straightforward characterization of the domain size, although any other composition can be used. (The NP localization and adsorption energy at the interface are governed by the NP and the PMMA−PS interfacial tension only.) The PMMA and PS molecular weights, 87 and 571 kDa, respectively, were selected to ensure that the two polymers have nearly the same zero shear viscosity at the annealing temperature ($\eta_{PS}/\eta_{PMMA} \sim 4$; see Figure S1). The blends were prepared by the rapid precipitation of homogeneous polymer blend solutions in nonsolvent baths.[59] This traps the phase-separation process in an early stage (before significant coarsening takes place), allowing the investigation of any annealing-induced coarsening phenomena. Annealing was performed under vacuum at 190 °C for different times and the resulting morphologies were characterized by

https://dx.doi.org/10.1021/acs.macromol.0c02108
Macromolecules 2020, 53, 10330−10338

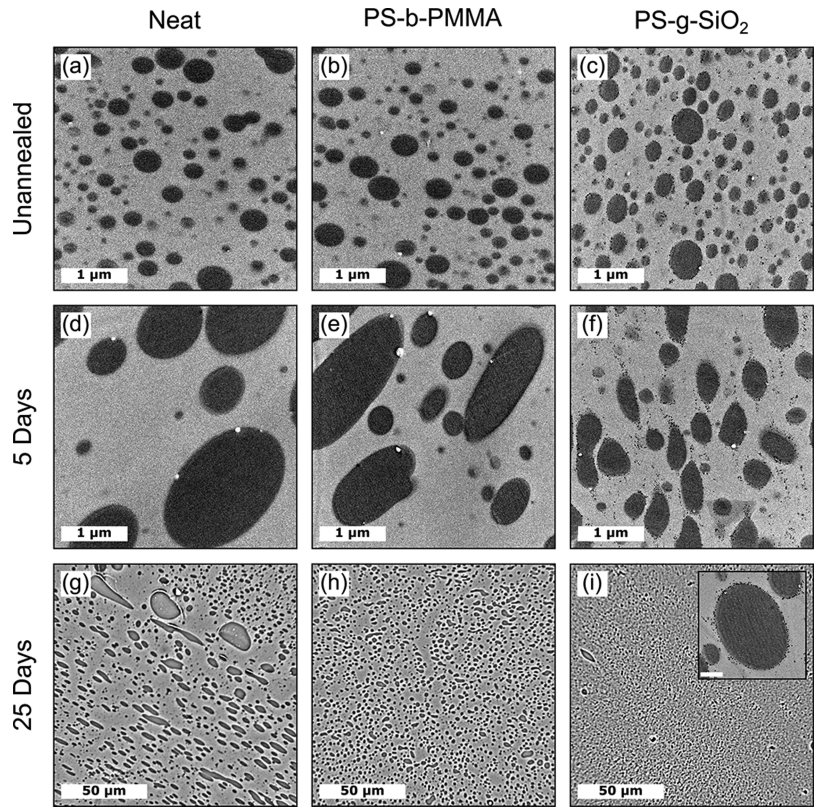

Figure 4. Micrographs showing the morphology evolution of neat (a,d,g), PS-*b*-PMMA-filled (b,e,h), and PS-*g*-SiO_2-filled (c,f,i) PMMA/PS (80/20) blends after static annealing for the designated periods (left). The compatibilizer loadings are 0.5 vol %. Brighter phase is PMMA, and darker one is PS. Scale bar for the inset in (i) is 250 nm.

Table 1. Morphology Evolution of Neat and Stabilized PMMA/PS (80/20) Blends after Static Annealing at 190 °C for Different Periods

		[a]droplet diameter (D_n) (nm)			[a]dispersity index (D_v/D_n)		
blend	compatibilizer (vol %)	unannealed	5 days	25 days	unannealed	5 days	25 days
PMMA/PS	0.0	222	656	3161	2.06	3.07	2.37
PMMA/PS/PS-*b*-PMMA	0.5	214	657	1921	2.07	2.59	1.86
PMMA/PS/PS-*g*-SiO_2	0.5	208	444	455	2.18	2.00	1.94
PMMA/PS/PS-*g*-SiO_2	5.0	173	192		1.30	1.37	

[a]Calculated based on the real droplet size distribution: $D_n = \sum n_i D_i / \sum n_i$ and $D_v = \sum n_i D_i^4 / \sum n_i D_i^3$, where n_i is the number of droplets having diameter D_i. The droplet dispersity index (PDI) is calculated as D_v/D_n.

TEM and phase-contrast optical microscopy. As controls, we prepared neat blends and blends filled with a symmetric PS-*b*-PMMA diblock copolymer (M_w^{total} = 104 kDa, $M_w/M_n \approx 1.09$) using the same technique. The latter is known to be an excellent compatibilizer for PMMA/PS blends.[4−6]

Figure 4 shows the morphology evolution of the blends after 5 and 25 days of annealing. The corresponding number average droplet diameters (D_n) and dispersity indices (PDIs) are shown in Table 1. The observed directionality in these micrographs is likely an artifact of ultramicrotomy because of the large compression forces involved (i.e., the stretching of the thin sections in the direction of cutting). Initially, all the blends have approximately the same D_n and PDI, demonstrating the effectiveness of the rapid precipitation method in quenching the system. The neat blend developed the largest domains and broadest dispersity after annealing, increasing in size from 222 to 3161 nm after 25 days (Figure 4g). In fact, the neat morphology varied significantly across the sample, which complicated the size distribution analysis—Figure 4g shows at least three different domain size ranges in a 140 × 140 μm area. The estimated PDI of this sample (≈2.37) is therefore a lower bound because of the neglect of some of the very large and likely some of the very small droplets in the analysis. The irregular droplet shapes are probably because of the uninterrupted coalescence phenomena taking place. Similarly, the droplet diameter of the diblock copolymer-filled blend increased from 214 to 1921 nm, but the resulting morphology was very regular (Figure 4h). The best improvement by far was seen in the PS-grafted SiO_2-filled blend, whose mean domain size increased from 208 to 455 nm (Figure 4i). Because both compatibilized systems have the same initial (as-quenched) PS domain size, the differences in the domain sizes upon annealing are attributed to the compatibilizers' stabilization efficiency.

The most striking aspect of the PS-grafted SiO_2-compatibilized system is that its domain size essentially remained unchanged between 5 and 25 days of annealing. This suggests that at around 5 days of annealing, the PMMA−PS interfacial

https://dx.doi.org/10.1021/acs.macromol.0c02108
Macromolecules 2020, 53, 10330−10338

area reduced to a degree at which the droplet coverage by the NPs (τ) became sufficient to significantly suppress further coalescence. To obtain an estimate of τ, we can approximate the NP packing at the interface as that of circles on a two-dimensional surface and normalize their total surface area, $S_{NP} = \frac{\phi_{NP}}{4/3\pi r^3}\pi r_{eff}^2$, by the total surface area of the PS droplets, $S_{PS} = \frac{\phi_{PS}}{1/6\pi D_n^3}\pi D_n^2$, giving[60,61]

$$\tau = \frac{D_n}{8}\left(\frac{r_{eff}^2}{r^3}\right)\left(\frac{\phi_{NP}}{\phi_{PS}}\right) \quad (3)$$

where r_{eff} is the effective NP radius after including the thickness of the brush and ϕ_{PS} and ϕ_{NP} are the PS and NP (core) volume fractions, respectively. For σ = 0.02 chains/nm^2 and M_n = 110 kDa, a simple geometric argument[62] shows that $r_{eff} \approx 9.5$ nm, that is, the brush has a thickness of about 2.5 nm. The maximum theoretical coverage for a monolayer of NPs, $\tau_{HCP} \approx 0.907$, corresponding to the hexagonal packing density of circles, is attained only when $D_n \approx 1060$ nm. Clearly, such extensive coalescence was not observed because the domains are about half as large, $D_n \approx 455$ nm ($\tau \approx 0.39$). This is corroborated by the inset in Figure 4i, which shows the existence of uncovered interfacial areas. The origin of this stabilization is unclear at present; we conjecture that at higher droplet coverages, the grafted NPs create a gel network around the droplet that resists further domain coalescence at the time scales considered here. Such "gel-like" behavior has been reported for polymers filled with well-dispersed[63] and percolating NP morphologies.[64]

We also prepared a similar PMMA/PS system with 5 vol % NP loading to investigate the change in τ (Figure 5). The

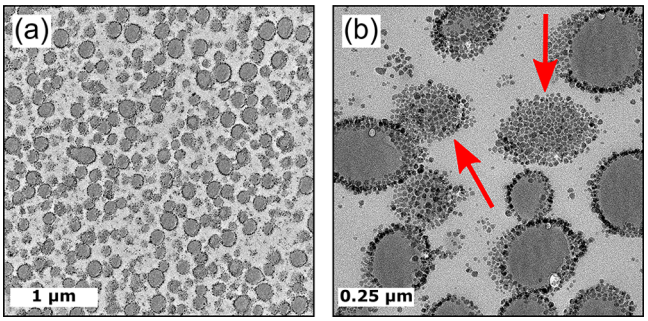

Figure 5. TEM micrographs of unannealed PMMA/PS (80/20) with 5 vol % PS-*g*-SiO_2 NPs at low- (a) and high magnification (b). Brighter phase is PMMA, and darker one is PS.

number-average droplet diameter D_n and the coverage τ for the unannealed blend are, respectively, 173 nm and 1.34, indicating the formation of more than a monolayer of NPs at the interface, as shown in the high-magnification micrograph (Figure 5b). More interestingly, because the average droplet size is close to the TEM specimen thickness (~60 nm), some droplets are cut far from their centers, as indicated by the arrows in Figure 5b—apparently, the droplets are protected by a near core−core packing of NPs. This is presumably a result of the conformational freedom afforded to the grafts in the low-grafting density regime.[65] The suppression of domain coalescence is confirmed by the 5-day annealing experiment (Table 1), which shows a negligible increase in the domain size to $D_n \approx 192$ nm ($\tau \approx 1.49$).

Comparison to Past Work. Although the PMMA/PS system is well studied in the literature, a direct comparison of compatibilizer efficiency is complicated by the varying preparation methods and experimental conditions. Walther et al.[11] adopted a melt mixing approach to investigate the PMMA domains in 20/80 (PMMA/PS) blends compatibilized with Janus NPs. They found comparable domain sizes to ours: D_n ranging from 710 to 125 nm for NP loadings between 0.5 and 5 vol %, respectively. Bryson et al.[12] used a similar Janus NP to investigate the morphologies of solvent-cast PMMA/PS blends. They observed larger domains, $D_n \approx 1$ μm at 8.0 vol % NP loading, although their blend composition, 56/44 (PMMA/PS), was different from ours. Similarly, Yoo et al.[38] observed a reduction in the domain size of solvent-cast 50/50 (PMMA/PS) blends from 920 to 320 nm with the addition of 10 wt % of Au NPs densely grafted with a poly(styrene-*b*-azido-polystyrene) (PS-*b*-PS-N_3) block copolymer, where the inner PS-N_3 blocks were cross-linked to improve the thermal stability of the Au−thiol bond. Because these domains are larger than what we observed in this study, we conjecture that the bulk of the coarsening phenomena in these compatibilized, solvent-cast blends occurred during solvent evaporation. By contrast, the rapid quenching of our blends in mechanically agitated nonsolvent baths froze the domains earlier in the phase-separation process,[59] allowing us to stabilize domains comparable in size to the ones obtained by melt-mixing[11] at relatively low loading. Clearly, the preparation method is an important factor in the stabilization efficiency of these compatibilizers, a phenomenon that we explain below.

Solvent-Cast PMMA/PS/PS-*g*-SiO_2 Blends. We prepared a PMMA/PS (80/20) blend filled with 0.5 vol % of our sparsely grafted PS-*g*-SiO_2 NPs by solvent-evaporation-induced demixing. The blend was solvent-cast from a dilute toluene solution, and the solvent was allowed to evaporate over a ~24 h period. The optical micrograph in Figure 6a shows the

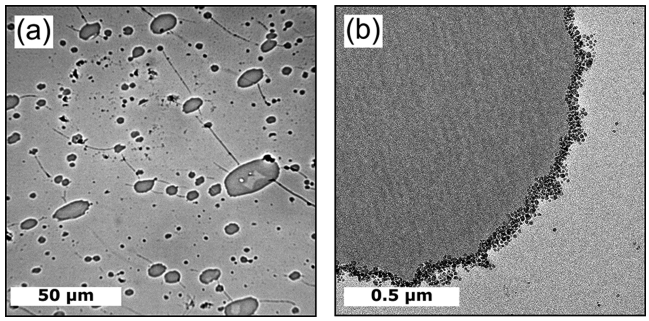

Figure 6. Micrographs of solvent-cast PMMA/PS (80/20) with 0.5 vol % PS-*g*-SiO_2 NPs at low- (a) and high-magnification (b). Brighter phase is PMMA, and darker one is PS.

formation of micrometer-sized domains, in sharp contrast to the highly stable 455 nm domains that we obtained by rapidly quenching the system and annealing in the melt state.

The origin of this discrepancy emphasizes the dominant role that the solvent plays in forming these morphologies. As the solvent is removed, the total polymer concentration (c) increases and eventually reaches a critical demixing concentration (c_K) at which phase separation occurs. Broseta et al.[66] showed that far from the critical point of demixing and in the limit of infinitely long chains, the interfacial tension of a

https://dx.doi.org/10.1021/acs.macromol.0c02108
Macromolecules 2020, 53, 10330−10338

polymer/polymer/solvent system depends on the total polymer concentration as follows

$$\gamma_{12}^{\infty} = \frac{kT}{\xi^2}\sqrt{\frac{u}{6}} \sim c^{1.65} \quad (4)$$

where the interfacial tension expression is analogous to the self-consistent field theory of Helfand and Tagami[67,68] with u ($\sim c^{0.3}$) being the effective monomer A−monomer B interaction parameter and ξ ($\sim c^{-0.75}$) being the correlation length of concentration fluctuations. Thus, the interfacial tension in the vicinity of c_K is nearly zero, and it increases with continued solvent evaporation. This suggests that the NPs are not firmly fixed at the interface near c_K because the free energy of adsorption depends on the interfacial tension as $\sim\gamma_{12}$.[25] It is also very likely that the NP localization in the demixed solution is different from that in the melt state, that is, when the five interfacial tensions in eq 2 vary differently with polymer concentration. Therefore, regardless of the NP stabilization efficiency in the melt, significant coarsening could occur in solution near c_K because of favorable kinetics and weak to nonexistent NP adsorption.

An interesting feature of these solvent-cast blends is the (occasional) formation of dense NP multilayers at the interfaces (Figure 6b). The near core−core packing of the NPs is again attributed to their low grafting density. The prevalence of these multilayers varied across the sample, but they were generally more pronounced in regions where significant coarsening occurred. This likely points to a major role played by coalescence in their formation, presumably through reducing the total PMMA−PS interfacial area to a degree much lower than the total surface area of the NPs. Because the critical demixing concentration varies with the molecular weight of the components like $c_K \sim M_w^{-0.62}$,[69] the solution demixes at a lower c_K for higher molecular weights. For such systems, one might expect to form more NP multilayers because of extended coarsening. Quantitative measurements for the domain sizes and the number of NP layers were difficult to perform because of considerable variation across the sample. Tsige and Grest[70] used computer simulations to show that the polymer concentration near the film−air interface increases sharply during solvent evaporation, creating a barrier for further solvent evaporation from deeper within the film. Therefore, the domain size and multilayer variations are likely because of a polymer concentration gradient across the film thickness during solvent evaporation. Evidently, these multilayer structures are inaccessible by melt preparation, at least over practical time scales. However, better control of the evaporation-induced phase separation is needed to obtain fine droplets with monodisperse NP multilayers.

CONCLUSIONS

In summary, silica NPs were designed to localize at immiscible PMMA−PS interfaces by sparsely grafting their surface (σ = 0.02 chains/nm^2) with long PS chains (M_n = 110 kDa). The resulting NPs strongly segregated to the interface and stabilized 455 nm PS domains at a low NP loading of 0.5 vol %; evidently, partial droplet coverage was enough to halt droplet coalescence in the melt over practical time scales. We showed that the blends stabilized by these NPs far outperform the ones compatibilized with a conventional diblock copolymer in terms of droplet size and stability against coalescence. Moreover, we demonstrated that these sparsely grafted NPs could achieve a dense, near core−core packing at the interface. We conjecture that this is a result of the conformational freedom the grafts experience at such low grafting densities. Thus, by carefully tuning the grafting parameters and the preparation method, we were able to obtain a fine morphology comparable to that produced by melt mixing. We also showed that solvent evaporation-induced phase separation provides access to densely packed NP multilayer structures at the interface; apparently, these structures form because of domain coalescence phenomena occurring in solution.

ASSOCIATED CONTENT

Supporting Information

The Supporting Information is available free of charge at https://pubs.acs.org/doi/10.1021/acs.macromol.0c02108.

Experimental details, image analysis details, interfacial tension estimation, and polymer viscosities (PDF)

AUTHOR INFORMATION

Corresponding Author

Sanat K. Kumar − *Department of Chemical Engineering, Columbia University, New York, New York 10027, United States;* orcid.org/0000-0002-6690-2221; Email: sk2794@columbia.edu

Authors

Husam Alkhodairi − *Department of Chemical Engineering, Columbia University, New York, New York 10027, United States;* orcid.org/0000-0002-3106-9129

Sebastian T. Russell − *Department of Chemical Engineering, Columbia University, New York, New York 10027, United States;* orcid.org/0000-0001-5322-492X

Julia Pribyl − *Department of Chemistry, University of South Carolina, Columbia, South Carolina 29208, United States;* orcid.org/0000-0002-9854-2849

Brian C. Benicewicz − *Department of Chemistry, University of South Carolina, Columbia, South Carolina 29208, United States;* orcid.org/0000-0003-4130-1232

Complete contact information is available at: https://pubs.acs.org/10.1021/acs.macromol.0c02108

Notes

The authors declare no competing financial interest.

ACKNOWLEDGMENTS

Financial support for this work was provided by the National Science Foundation under grants DMR-1709061 (S.K.K.) and DMREF-1629052 (B.C.B., J.P.). We gratefully acknowledge the use of SEMC-NYSBC facilities for ultramicrotomy work. We thank Professor Basil Favis for many helpful discussions.

REFERENCES

(1) Koning, C. Strategies for compatibilization of polymer blends. *Prog. Polym. Sci.* **1998**, *23*, 707−757.

(2) Anastasiadis, S. H.; Gancarz, I.; Koberstein, J. T. Compatibilizing effect of block copolymers added to the polymer/polymer interface. *Macromolecules* **1989**, *22*, 1449−1453.

(3) Shull, K. R.; Kramer, E. J.; Hadziioannou, G.; Tang, W. Segregation of block copolymers to interfaces between immiscible homopolymers. *Macromolecules* **1990**, *23*, 4780−4787.

(4) Thomas, S.; Prud'homme, R. E. Compatibilizing effect of block copolymers in heterogeneous polystyrene/poly(methyl methacrylate) blends. *Polymer* **1992**, *33*, 4260−4268.

(5) Macosko, C. W.; Guégan, P.; Khandpur, A. K.; Nakayama, A.; Marechal, P.; Inoue, T. Compatibilizers for Melt Blending: Premade Block Copolymers. *Macromolecules* **1996**, *29*, 5590−5598.
(6) Jeon, H. K.; Zhang, J.; Macosko, C. W. Premade vs. reactively formed compatibilizers for PMMA/PS melt blends. *Polymer* **2005**, *46*, 12422−12429.
(7) Sundararaj, U.; Macosko, C. W. Drop Breakup and Coalescence in Polymer Blends: The Effects of Concentration and Compatibilization. *Macromolecules* **1995**, *28*, 2647−2657.
(8) Lyu, S.; Jones, T. D.; Bates, F. S.; Macosko, C. W. Role of Block Copolymers on Suppression of Droplet Coalescence. *Macromolecules* **2002**, *35*, 7845−7855.
(9) Galloway, J. A.; Jeon, H. K.; Bell, J. R.; Macosko, C. W. Block copolymer compatibilization of cocontinuous polymer blends. *Polymer* **2005**, *46*, 183−191.
(10) Creton, C.; Kramer, E. J.; Hui, C. Y.; Brown, H. R. Failure mechanisms of polymer interfaces reinforced with block copolymers. *Macromolecules* **1992**, *25*, 3075−3088.
(11) Walther, A.; Matussek, K.; Müller, A. H. E. Engineering Nanostructured Polymer Blends with Controlled Nanoparticle Location using Janus Particles. *ACS Nano* **2008**, *2*, 1167−1178.
(12) Bryson, K. C.; Löbling, T. I.; Müller, A. H. E.; Russell, T. P.; Hayward, R. C. Using Janus Nanoparticles To Trap Polymer Blend Morphologies during Solvent-Evaporation-Induced Demixing. *Macromolecules* **2015**, *48*, 4220−4227.
(13) Bahrami, R.; Löbling, T. I.; Gröschel, A. H.; Schmalz, H.; Müller, A. H. E.; Altstädt, V. The Impact of Janus Nanoparticles on the Compatibilization of Immiscible Polymer Blends under Technologically Relevant Conditions. *ACS Nano* **2014**, *8*, 10048−10056.
(14) Chung, H.-j.; Ohno, K.; Fukuda, T.; Composto, R. J. J. Self-Regulated Structures in Nanocomposites by Directed Nanoparticle Assembly. *Nano Lett.* **2005**, *5*, 1878−1882.
(15) Gam, S.; Corlu, A.; Chung, H.-J.; Ohno, K.; Hore, M. J. A.; Composto, R. J. A jamming morphology map of polymer blend nanocomposite films. *Soft Matter* **2011**, *7*, 7262.
(16) Chung, H.-J.; Kim, J.; Ohno, K.; Composto, R. J. J. Controlling the Location of Nanoparticles in Polymer Blends by Tuning the Length and End Group of Polymer Brushes. *ACS Macro Lett.* **2012**, *1*, 252−256.
(17) Kang, D. J.; Kwon, T.; Kim, M. P.; Cho, C.-H.; Jung, H.; Bang, J.; Kim, B. J. Creating Opal-Templated Continuous Conducting Polymer Films with Ultralow Percolation Thresholds Using Thermally Stable Nanoparticles. *ACS Nano* **2011**, *5*, 9017−9027.
(18) Kwon, T.; Kim, T.; Ali, F. B.; Kang, D. J.; Yoo, M.; Bang, J.; Lee, W.; Kim, B. J. Size-Controlled Polymer-Coated Nanoparticles as Efficient Compatibilizers for Polymer Blends. *Macromolecules* **2011**, *44*, 9852−9862.
(19) Huang, S.; Bai, L.; Trifkovic, M.; Cheng, X.; Macosko, C. W. Controlling the Morphology of Immiscible Cocontinuous Polymer Blends via Silica Nanoparticles Jammed at the Interface. *Macromolecules* **2016**, *49*, 3911−3918.
(20) Elias, L.; Fenouillot, F.; Majeste, J. C.; Cassagnau, P. Morphology and rheology of immiscible polymer blends filled with silica nanoparticles. *Polymer* **2007**, *48*, 6029−6040.
(21) Vandebril, S.; Vermant, J.; Moldenaers, P. Efficiently suppressing coalescence in polymer blends using nanoparticles: role of interfacial rheology. *Soft Matter* **2010**, *6*, 3353.
(22) Jalali Dil, E.; Virgilio, N.; Favis, B. D. The effect of the interfacial assembly of nano-silica in poly(lactic acid)/poly(butylene adipate-co-terephthalate) blends on morphology, rheology and mechanical properties. *Eur. Polym. J.* **2016**, *85*, 635−646.
(23) Parpaite, T.; Otazaghine, B.; Taguet, A.; Sonnier, R.; Caro, A. S.; Lopez-Cuesta, J. M. Incorporation of modified Stöber silica nanoparticles in polystyrene/polyamide-6 blends: Coalescence inhibition and modification of the thermal degradation via controlled dispersion at the interface. *Polymer* **2014**, *55*, 2704−2715.
(24) Palacios, J. K.; Sangroniz, A.; Eguiazabal, J. I.; Etxeberria, A.; Müller, A. J. Tailoring the properties of PP/PA6 nanostructured blends by the addition of nanosilica and compatibilizer agents. *Eur. Polym. J.* **2016**, *85*, 532−552.
(25) Binks, B. P. Particles as surfactants—similarities and differences. *Curr. Opin. Colloid Interface Sci.* **2002**, *7*, 21−41.
(26) Akcora, P.; Liu, H.; Kumar, S. K.; Moll, J.; Li, Y.; Benicewicz, B. C.; Schadler, L. S.; Acehan, D.; Panagiotopoulos, A. Z.; Pryamitsyn, V.; Ganesan, V.; Ilavsky, J.; Thiyagarajan, P.; Colby, R. H.; Douglas, J. F. Anisotropic self-assembly of spherical polymer-grafted nanoparticles. *Nat. Mater.* **2009**, *8*, 354−359.
(27) Bockstaller, M. R.; Lapetnikov, Y.; Margel, S.; Thomas, E. L. Size-Selective Organization of Enthalpic Compatibilized Nanocrystals in Ternary Block Copolymer/Particle Mixtures. *J. Am. Chem. Soc.* **2003**, *125*, 5276−5277.
(28) Böker, A.; Lin, Y.; Chiapperini, K.; Horowitz, R.; Thompson, M.; Carreon, V.; Xu, T.; Abetz, C.; Skaff, H.; Dinsmore, A. D.; Emrick, T.; Russell, T. P. Hierarchical nanoparticle assemblies formed by decorating breath figures. *Nat. Mater.* **2004**, *3*, 302−306.
(29) Lin, Y.; Böker, A.; He, J.; Sill, K.; Xiang, H.; Abetz, C.; Li, X.; Wang, J.; Emrick, T.; Long, S.; Wang, Q.; Balazs, A.; Russell, T. P. Self-directed self-assembly of nanoparticle/copolymer mixtures. *Nature* **2005**, *434*, 55−59.
(30) Li, Q.; He, J.; Glogowski, E.; Li, X.; Wang, J.; Emrick, T.; Russell, T. P. Responsive Assemblies: Gold Nanoparticles with Mixed Ligands in Microphase Separated Block Copolymers. *Adv. Mater.* **2008**, *20*, 1462−1466.
(31) Lin, Y.; Daga, V. K.; Anderson, E. R.; Gido, S. P.; Watkins, J. J. Nanoparticle-Driven Assembly of Block Copolymers: A Simple Route to Ordered Hybrid Materials. *J. Am. Chem. Soc.* **2011**, *133*, 6513−6516.
(32) Chiu, J. J.; Kim, B. J.; Kramer, E. J.; Pine, D. J. Control of Nanoparticle Location in Block Copolymers. *J. Am. Chem. Soc.* **2005**, *127*, 5036−5037.
(33) Kim, B. J.; Bang, J.; Hawker, C. J.; Chiu, J. J.; Pine, D. J.; Jang, S. G.; Yang, S.-M.; Kramer, E. J. Creating Surfactant Nanoparticles for Block Copolymer Composites through Surface Chemistry. *Langmuir* **2007**, *23*, 12693−12703.
(34) Kim, B. J.; Bang, J.; Hawker, C. J.; Kramer, E. J. Effect of Areal Chain Density on the Location of Polymer-Modified Gold Nanoparticles in a Block Copolymer Template. *Macromolecules* **2006**, *39*, 4108−4114.
(35) Kim, B. J.; Fredrickson, G. H.; Hawker, C. J.; Kramer, E. J. Nanoparticle Surfactants as a Route to Bicontinuous Block Copolymer Morphologies. *Langmuir* **2007**, *23*, 7804−7809.
(36) Kim, B. J.; Fredrickson, G. H.; Kramer, E. J. Effect of Polymer Ligand Molecular Weight on Polymer-Coated Nanoparticle Location in Block Copolymers. *Macromolecules* **2008**, *41*, 436−447.
(37) Kim, B. J.; Fredrickson, G. H.; Bang, J.; Hawker, C. J.; Kramer, E. J. Tailoring Core−Shell Polymer-Coated Nanoparticles as Block Copolymer Surfactants. *Macromolecules* **2009**, *42*, 6193−6201.
(38) Yoo, M.; Kim, S.; Lim, J.; Kramer, E. J.; Hawker, C. J.; Kim, B. J.; Bang, J. Facile Synthesis of Thermally Stable Core−Shell Gold Nanoparticles via Photo-Cross-Linkable Polymeric Ligands. *Macromolecules* **2010**, *43*, 3570−3575.
(39) Jang, S. G.; Kim, B. J.; Hawker, C. J.; Kramer, E. J. Bicontinuous Block Copolymer Morphologies Produced by Interfacially Active, Thermally Stable Nanoparticles. *Macromolecules* **2011**, *44*, 9366−9373.
(40) Jang, S. G.; Khan, A.; Dimitriou, M. D.; Kim, B. J.; Lynd, N. A.; Kramer, E. J.; Hawker, C. J. Synthesis of thermally stable Au-core/Pt-shell nanoparticles and their segregation behavior in diblock copolymer mixtures. *Soft Matter* **2011**, *7*, 6255.
(41) Jang, S. G.; Kramer, E. J.; Hawker, C. J. Controlled Supramolecular Assembly of Micelle-Like Gold Nanoparticles in PS-b -P2VP Diblock Copolymers via Hydrogen Bonding. *J. Am. Chem. Soc.* **2011**, *133*, 16986−16996.
(42) Kwon, T.; Ku, K. H.; Kang, D. J.; Lee, W. B.; Kim, B. J. Aspect-Ratio Effect of Nanorod Compatibilizers in Conducting Polymer Blends. *ACS Macro Lett.* **2014**, *3*, 398−404.

https://dx.doi.org/10.1021/acs.macromol.0c02108
Macromolecules 2020, 53, 10330−10338

(43) Kumar, S. K.; Jouault, N.; Benicewicz, B.; Neely, T. Nanocomposites with Polymer Grafted Nanoparticles. *Macromolecules* **2013**, *46*, 3199−3214.
(44) Asai, M.; Zhao, D.; Kumar, S. K. Accurate estimation of the polymer coverage of hairy nanoparticles. *Soft Matter* **2018**, *14*, 7906−7915.
(45) Leibler, L.; Ajdari, A.; Mourran, A.; Coulon, G.; Chatenay, D. *Ordering in Macromolecular Systems*; Springer: Berlin, Heidelberg, 1994; pp 301−311.
(46) Ferreira, P. G.; Ajdari, A.; Leibler, L. Scaling Law for Entropic Effects at Interfaces between Grafted Layers and Polymer Melts. *Macromolecules* **1998**, *31*, 3994−4003.
(47) Shull, K. R. Wetting autophobicity of polymer melts. *Faraday Discuss.* **1994**, *98*, 203.
(48) Walther, A.; Müller, A. H. E. Janus Particles: Synthesis, Self-Assembly, Physical Properties, and Applications. *Chem. Rev.* **2013**, *113*, 5194−5261.
(49) Kango, S.; Kalia, S.; Celli, A.; Njuguna, J.; Habibi, Y.; Kumar, R. Surface modification of inorganic nanoparticles for development of organic−inorganic nanocomposites—A review. *Prog. Polym. Sci.* **2013**, *38*, 1232−1261.
(50) Li, C.; Han, J.; Ryu, C. Y.; Benicewicz, B. C. A Versatile Method To Prepare RAFT Agent Anchored Substrates and the Preparation of PMMA Grafted Nanoparticles. *Macromolecules* **2006**, *39*, 3175−3183.
(51) Midya, J.; Rubinstein, M.; Kumar, S. K.; Nikoubashman, A. Structure of Polymer-Grafted Nanoparticle Melts. *ACS Nano* **2020**, DOI: 10.1021/acsnano.0c06134.
(52) Landry, C. J. T.; Coltrain, B. K.; Wesson, J. A.; Zumbulyadis, N.; Lippert, J. L. In situ polymerization of tetraethoxysilane in polymers: chemical nature of the interactions. *Polymer* **1992**, *33*, 1496−1506.
(53) Srivastava, S.; Agarwal, P.; Archer, L. A. Tethered Nanoparticle−Polymer Composites: Phase Stability and Curvature. *Langmuir* **2012**, *28*, 6276−6281.
(54) Hasegawa, R.; Aoki, Y.; Doi, M. Optimum Graft Density for Dispersing Particles in Polymer Melts. *Macromolecules* **1996**, *29*, 6656−6662.
(55) Owens, D. K.; Wendt, R. C. Estimation of the surface free energy of polymers. *J. Appl. Polym. Sci.* **1969**, *13*, 1741−1747.
(56) Carriere, C. J.; Cohen, A.; Arends, C. B. Estimation of Interfacial Tension Using Shape Evolution of Short Fibers. *J. Rheol.* **1989**, *33*, 681−689.
(57) Kim, B.; Ryu, D. Y.; Pryamitsyn, V.; Ganesan, V. Dewetting of PMMA on PS−Brush Substrates. *Macromolecules* **2009**, *42*, 7919−7923.
(58) Lee, H.; Lee, W.; Soo Han, Y.; Kim, E.; Ryu, D. Y. Autophobic dewetting of polystyrenes on the substrates grafted with chemically identical polymers. *Polym. J.* **2016**, *48*, 503−507.
(59) Lee, J.; Han, C. Evolution of a dispersed morphology from a co-continuous morphology in immiscible polymer blends. *Polymer* **1999**, *40*, 2521−2536.
(60) Arditty, S.; Whitby, C. P.; Binks, B. P.; Schmitt, V.; Leal-Calderon, F. Some general features of limited coalescence in solid-stabilized emulsions. *Eur. Phys. J. E: Soft Matter Biol. Phys.* **2003**, *11*, 273−281.
(61) Herzig, E. M.; White, K. A.; Schofield, A. B.; Poon, W. C. K.; Clegg, P. S. Bicontinuous emulsions stabilized solely by colloidal particles. *Nat. Mater.* **2007**, *6*, 966−971.
(62) Jimenez, A. M.; Krauskopf, A. A.; Pérez-Camargo, R. A.; Zhao, D.; Pribyl, J.; Jestin, J.; Benicewicz, B. C.; Müller, A. J.; Kumar, S. K. Effects of Hairy Nanoparticles on Polymer Crystallization Kinetics. *Macromolecules* **2019**, *52*, 9186−9198.
(63) Chen, Q.; Gong, S.; Moll, J.; Zhao, D.; Kumar, S. K.; Colby, R. H. Mechanical Reinforcement of Polymer Nanocomposites from Percolation of a Nanoparticle Network. *ACS Macro Lett.* **2015**, *4*, 398−402.
(64) Akcora, P.; Kumar, S. K.; Moll, J.; Lewis, S.; Schadler, L. S.; Li, Y.; Benicewicz, B. C.; Sandy, A.; Narayanan, S.; Ilavsky, J.; Thiyagarajan, P.; Colby, R. H.; Douglas, J. F. "Gel-like" Mechanical Reinforcement in Polymer Nanocomposite Melts. *Macromolecules* **2010**, *43*, 1003−1010.
(65) Bozorgui, B.; Meng, D.; Kumar, S. K.; Chakravarty, C.; Cacciuto, A. Fluctuation-Driven Anisotropic Assembly in Nanoscale Systems. *Nano Lett.* **2013**, *13*, 2732−2737.
(66) Broseta, D.; Leibler, L.; Ould Kaddour, L.; Strazielle, C. A theoretical and experimental study of interfacial tension of immiscible polymer blends in solution. *J. Chem. Phys.* **1987**, *87*, 7248−7256.
(67) Helfand, E.; Tagami, Y. Theory of the interface between immiscible polymers. *J. Polym. Sci., Part B: Polym. Lett.* **1971**, *9*, 741−746.
(68) Helfand, E.; Tagami, Y. Theory of the Interface between Immiscible Polymers. II. *J. Chem. Phys.* **1972**, *56*, 3592−3601.
(69) Broseta, D.; Leibler, L.; Joanny, J. F. Critical properties of incompatible polymer blends dissolved in a good solvent. *Macromolecules* **1987**, *20*, 1935−1943.
(70) Tsige, M.; Grest, G. S. Solvent evaporation and interdiffusion in polymer films. *J. Phys.: Condens. Matter* **2005**, *17*, S4119−S4132.

https://dx.doi.org/10.1021/acs.macromol.0c02108
Macromolecules 2020, 53, 10330−10338